Available online at www.sciencedirect.com
ScienceDirect
Polymer 48 (2007) 6707–6718
polymer
www.elsevier.com/locate/polymer

Synthesis of poly(*N*-isopropylacrylamide) copolymer containing anhydride and imide comonomers – A theoretical study on reversal of LCST

Raju Francis [a,*], C.P. Jijil [a], C. Achutha Prabhu [b], C.H. Suresh [b,**]

[a] *Post Graduate and Research Department of Chemistry, St. Joseph's College, Devagiri, Calicut 673008, Kerala, India*
[b] *Computational Modeling and Simulation Section, National Institute for Interdisciplinary Science and Technology (CSIR), Trivandrum 695019, Kerala, India*

Received 7 July 2007; received in revised form 24 August 2007; accepted 25 August 2007
Available online 5 September 2007

Abstract

The stimuli sensitive copolymer NIPAM-*co*-MI was prepared by copolymerizing NIPAM (*N*-isopropylacrylamide) with varying concentrations of maleimide (MI). The copolymer showed the same ratio of the monomeric components as that of the initial monomer feed ratio, with the two components arranged in the chain in a purely random sequence. Interestingly, the lower critical solution temperature (LCST) of NIPAM-*co*-MI was found to decrease with increase in MI loading in the copolymer. This behavior was in drastic contrast to the LCST behavior of a similar copolymer NIPAM-*co*-MA of NIPAM and maleic anhydride (MA) where the LCST showed an increase with increase in the MA concentration. A theoretical interpretation of the contrasting LCST behavior of both NIPAM-*co*-MI and NIPAM-*co*-MA was obtained by quantum mechanical (QM) modeling on small structural units of the polymers as well as molecular dynamic (MD) simulations at LCST and above the LCST on 50-unit oligomer model of the polymers. The QM models showed that the MI based polymer is more inclined towards bend structure, higher hydration, and higher intramolecular hydrogen bond formation between its monomer units when compared to those of the MA based polymer. The results of the large scale MD simulation was in complete support of the QM results as it showed the formation of a more folded and highly hydrated NIPAM-*co*-MI than NIPAM-*co*-MA.

Keywords: Lower critical solution temperature; *N*-Isopropylacrylamide; Molecular dynamics

1. Introduction

It is well known that *N*-isopropylacrylamide (NIPAM) based polymers (homo, block, graft, dendrimer, star, etc.) show clouding point (or lower critical solution temperature (LCST)) in aqueous solution and the value varies with pH, nature of comonomer and average molecular weight of polymer, in general [1,2]. This made its extensive study and use in the development of mainly drug delivery vehicles and hydrogels [3]. The unusual thermal behavior of PNIPAM is the abrupt transition (coil to globule) from a hydrophilic to a hydrophobic peripheral structure at the clouding point (LCST). This value was found to lie between 30 and 35 °C depending on the detailed microstructure of the polymer [1].

Generally a comonomer hydrophilic than NIPAM increases the LCST of the copolymer and a hydrophobic comonomer causes a decrease in the LCST [4,5] and this property has been found useful in the case of recovery of solutes, catalysts [6] and for drug delivery. In literature it is confirmed that a hydrophilic coil to a hydrophobic globule transition of the polymer structure takes place at the LCST [7] and this intramolecular collapse has been studied in connection with some basic problems such as protein folding [8].

In the present study we report the role of maleimide units in controlling the LCST behavior of NIPAM copolymers. These results were then compared with the reported NIPAM-*co*-MA system [9]. Additionally, theoretical models comprising of the

* Corresponding author. Tel.: +91 495 2355901; fax: +91 495 2357370.
** Corresponding author. Tel.: +91 471 2515264; fax: +91 471 2491712.
E-mail addresses: rajufrancis@yahoo.com (R. Francis), sureshch@gmail.com (C.H. Suresh).

0032-3861/$ - see front matter © 2007 Elsevier Ltd. All rights reserved.
doi:10.1016/j.polymer.2007.08.061

basic structural units of both NIPAM-*co*-MI and NIPAM-*co*-MA have been constructed and studied at density functional level to explain the H-bonding interactions in the copolymer. Furthermore, to get a deeper understanding of the unexpected LCST behavior of these copolymers, molecular dynamic (MD) simulations have been carried out on 50-unit oligomer chains of the two copolymers in the presence of about 10,000 water molecules.

2. Experimental

2.1. Materials

N-Isopropylacrylamide (NIPAM) (Sigma–Aldrich) was purified before use by distillation followed by recrystallization from diethyl ether. α,α-Azobisisobutyronitrile (AIBN) (Spectrochem, India) was recrystallized from methanol just before use. Maleimide (MI) (MERCK) was synthesized according to the procedure reported in the literature [11]. Other solvents were purchased locally and purified by standard procedures before use.

2.2. Synthesis of NIPAM-co-MI

The required amount of monomers, solvent (1,4-dioxane) and initiator (AIBN) was taken in glass tubes (1.4 cm diameter and 10 cm long), stoppered with rubber septa. The polymerization mixture was deoxygenated for 15 min by purging with dry nitrogen and heated at 70 °C for known periods of time. The copolymers (Scheme 1) were precipitated by pouring the reaction mixtures into excess of diethyl ether. After two reprecipitations by pouring a dioxane solution into diethyl ether, the copolymers were dried in a vacuum desiccator at 35 °C.

2.3. Analytical methods

The IR spectrum of the copolymer was recorded in FT-IR spectrophotometer (Shimadzu). For NMR spectrum samples were dissolved in DMSO-d_6 and were scanned between δ 0 and 14 (Bruker). UV–vis spectrophotometer with temperature control (Shimadzu) was used to record the absorption spectrum of the copolymer and also to record the LCST point. Thus obtained LCST values were rechecked by manually recording the clouding point using an ordinary thermometer. The viscosity average molecular weight (M_v) of these polymers was obtained by time of flow method using polystyrene standards.

3. Results and discussion

3.1. Copolymer synthesis

The copolymerization of NIPAM and maleimide was carried out in 1,4-dioxane at 70 °C using AIBN as thermal initiator (Scheme 1). This copolymer was easily precipitated in diethyl ether as colourless powder. The parameters of a typical copolymerization reaction are presented in Table 1. 1,4-Dioxane was used as the solvent as the copolymer formed was insoluble in common solvents like THF, toluene, etc. The percentage conversion was calculated from the dried weight of the polymer and the initial total weight of the comonomers. ^{1}H NMR technique was used to deduce the copolymer composition by selectively integrating the signals at δ 7.7 corresponding to 'NH' proton in NIPAM and δ 11.1 corresponding to 'NH' proton in MI [9,12]. The portion of NMR signals showing relative variation with different copolymers is shown in Fig. 1. It shows relative increase in maleimide signals with increase in initial loading. The theoretical molecular weight presented in Table 1 is calculated by comparing the initiator and total monomer concentrations. The viscosity average molecular weight (M_v) determined by time of flow method was compared with the theoretical values. The comparison is poor as can be seen from Table 1 possibly due to uncontrolled radical polymerization reaction. The copolymer composition curve presented in Fig. 2 shows that the two monomers, viz. NIPAM and MI, showed no preference to be incorporated in the main chain during the reaction.

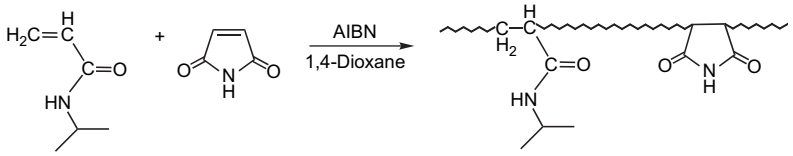

Scheme 1.

Table 1
The characteristics of copolymerization reaction of NIPAM with MI[a]

Run	Monomer feed (%)		Conversion (%)	Copolymer composition (%)		M_{nth}	M_v
	NIPAM	MI		NIPAM	MI		
1	90	10	77	90	10	2150	111,382
2	70	30	99	69	31	2684	52,253
3	50	50	85	47	53	2237	46,753

[a] Total monomer con. [M] = 10.2×10^{-3} mol, [AIBN] = 2% of [M], 1,4-dioxane = 6 mL, time = 25 min, temperature = 70 °C, M_{nth} = molecular weight (theoretical), M_v = molecular weight (viscosity).

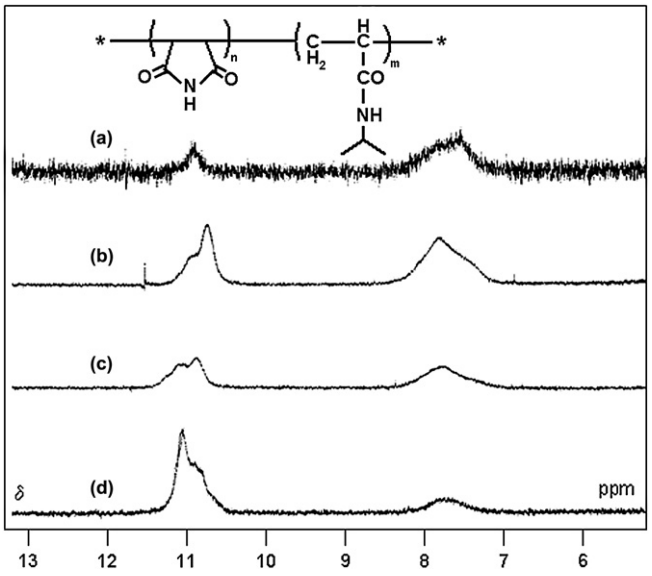

Fig. 1. A portion of the ^{1}H NMR spectra of NIPAM-*co*-MI copolymers showing peaks due to the two "NH" (imide and amide) signals; (a) 17, (b) 39, (c) 50 and (d) 80 are mole percentage of maleimide units in the copolymer.

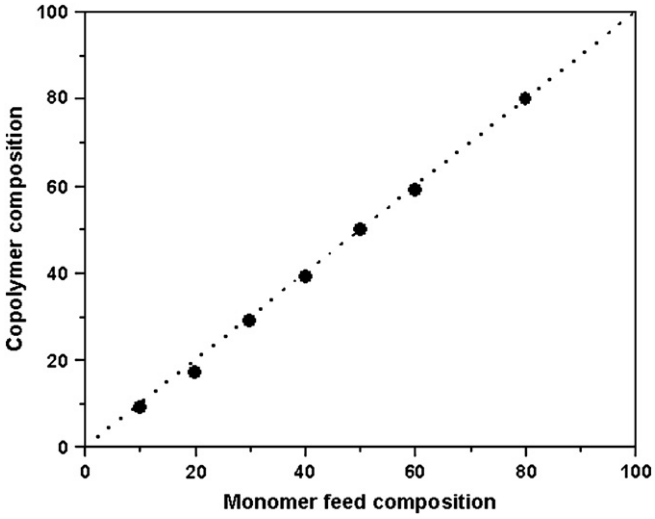

Fig. 2. Percentage composition of maleimide in the initial feed and copolymer obtained from ^{1}H NMR study.

3.1.1. Determination of lower critical solution temperature of copolymer

Among the solution properties of the copolymer the determination of lower critical solution temperature (LCST) in water was the main objective behind this report. The reported LCST of PNIPAM was found to be between 30 and 35 °C depending on the molecular weight. In addition, the LCST can vary with the nature of the comonomer incorporated in the main chain as discussed earlier [4]. It can be noted that the presence of a cyclic system induces restriction to chain flexibility.

A few samples of MA and NIPAM were prepared and the appearance of turbidity (LCST) in a buffer (acetic acid/sodium acetate) solution at pH = 4, was determined [13]. The LCST values in our system (NIPAM-*co*-MI) recorded by visual examination of turbidity are presented in Table 2. Interestingly the LCST, in the buffer solution at pH = 4, of the copolymer found to decrease with maleimide units in the main chain. It was also noted that beyond certain mol% (~30) of MI in the copolymer there was no recordable LCST behavior. This result of lowering of LCST is just opposite to the one obtained earlier in the case of NIPAM-*co*-MA copolymers (Fig. 3) [13]. Hence the probable reason for lowering of LCST could be chain stiffening along with intramolecular H-bonding. The intramolecular hydrogen bonding is formed between amide group in NIPAM and the imide portion in maleimide. Thus, in effect comparatively less number of amide units is available for solvent induced hydration. Hence in this case turbidity appears at a lower temperature.

Table 2
The effect of copolymer composition on LCST values of NIPAM-*co*-MI copolymers[a]

Percentage composition of maleimide in poly(NIPAM-*co*-MI) copolymer by ^{1}H NMR (%)	LCST of poly(NIPAM-*co*-MI) copolymer (°C)
9	28
17	24
29	15
39	Insoluble
50	Insoluble
59	Insoluble
80	Insoluble

[a] Buffer = sodium acetate/acetic acid, pH = 4.

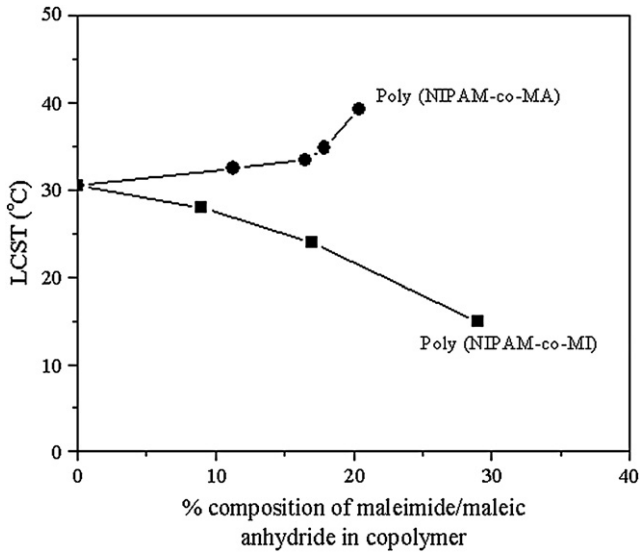

Fig. 3. Variation of LCST of poly(NIPAM-*co*-MA) [9] and poly(NIPAM-*co*-MI) with copolymer composition.

3.1.2. Effect of time and cycle of operations on LCST of copolymers

Additionally, the copolymer, which we prepared in this study, was compared with NIPAM-*co*-MA system studied by Kesim et al. for their stability in water [9]. The reproducibility in LCST value of NIPAM-*co*-MI and NIPAM-*co*-MA was

recorded at pH = 4 and 7. This variation in graphical format is presented in Fig. 4. In this figure Graphs (1) and (2) are recorded by taking the mean LCST of one cycle of cooling and heating analysis. This experiment proves the overall stability of these two systems when LCST value was noted after one cycle of heating and cooling analysis at least for the first few days. When it was raised to five cycles the same observation resulted, which confirmed its reproducibility and stability of the system. It was also noticed that there was approximately 3 °C difference between the heating and the cooling analysis for the LCST values as in the case of NIPAM-*co*-MI whereas only 1 °C was observed in the latter case. Thus it can be concluded from Fig. 4 that NIPAM-*co*-MI is stable at pH = 4, even for longer periods of time, whereas it is unstable at pH = 7 after few days. The variation in the case of NIPAM-*co*-MA can be explained based on the partial hydrolysis of anhydride moieties at pH = 4. Based on this it can be proposed that at pH = 7, the hydrolysis is very fast and reached the limiting point, 35 °C. But such an explanation in the case of NIPAM-*co*-MI is not valid as LCST value drops with time at pH = 7 (Fig. 4(2)). Detailed investigation and a reasonable explanation would be the subject matter of another paper.

3.2. Theoretical modeling

3.2.1. DFT calculations

The marked difference in the properties of NIPAM-*co*-MI and NIPAM-*co*-MA can be mainly attributed to the differences in the electronic properties of the MI and MA moieties as these two groups distinguish the two copolymers from one another. Although the replacement of −NH− segment of MI by O atom will give us the isoelectronic MA unit, the two moieties are fundamentally different in their electronic features. In the case of MI, the carbonyl groups and the NH bond are strong hydrogen bond (H-bond) acceptors and donor, respectively. On the other hand, in the case of MA, all the three oxygen atoms can only act as H-bond acceptors. Since, water can act both as a H-bond donor and as a H-bond acceptor, the hydration of MI and MA units is expected to show significant differences and which in turn will affect the LCST behavior. To get further insight into this issue, we have resorted to density functional theory (DFT) calculations on model molecules **1**−**4** (Fig. 5) relevant for defining the structures of NIPAM-*co*-MI and NIPAM-*co*-MA copolymers.

The DFT method of B3LYP/6-31 + G(d,p) is chosen for locating all the minimum energy conformations of molecular systems [14,15]. Further, to understand the electron distributions of systems **1** and **2**, the corresponding DFT wavefunctions are used to calculate the molecular electrostatic potential (MESP) [16,17]. For the interaction energy calculations, the supermolecule approach [18] is employed. The correction for the basis set super position error in the interaction energy calculations is determined by employing the procedure of Boys and Bernardi [19a]. All the DFT calculations have been done with Gaussian 03 suit of programs [19b].

*3.2.1.1. Electronic features of **1** and **2**.* MESP is often used as a convenient tool to understand the electron distribution,

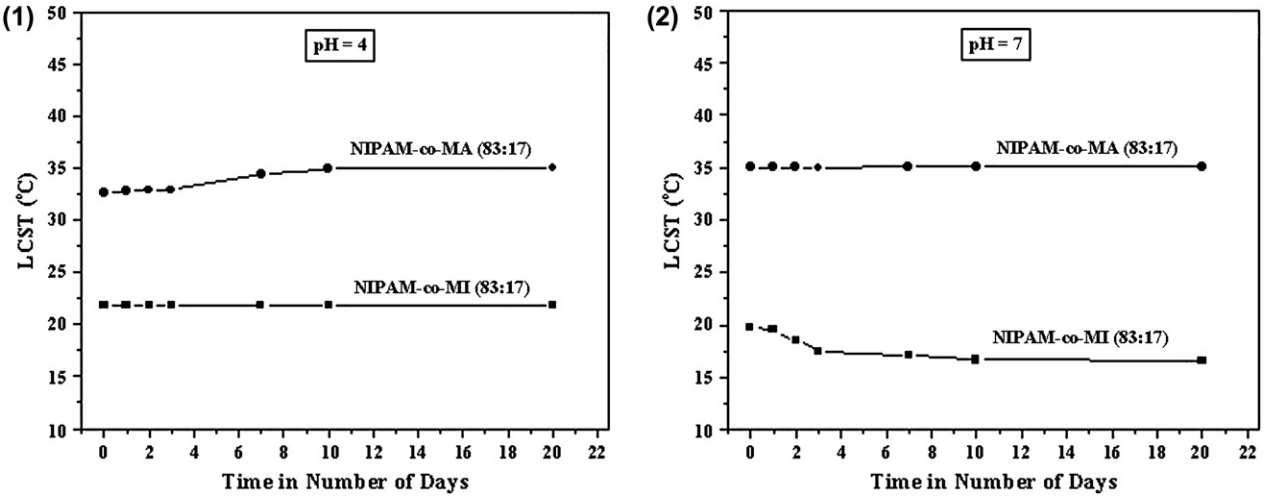

Fig. 4. Effect of time on LCST of NIPAM-*co*-MI and NIPAM-*co*-MA copolymer systems. Graphs (1) and (2) are plotted after one cycle and five cycles of heating and cooling analysis.

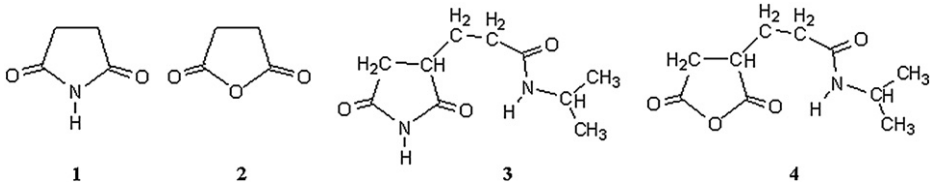

Fig. 5. Selected model molecules.

particularly the π-conjugation features, aromaticity, and lone pair strength of molecular systems [16,17,20–23]. In the present work, the MESP features of MI (**1**) and MA (**2**) units are calculated and their pictorial representation is depicted in Fig. 6. The carbonyl oxygen atom of MI unit has more negative potential than the carbonyl oxygen of MA unit. This result supports a higher strength for the H-bond interaction in the former compared to that of the latter. The red MESP region around the N–H hydrogen of MI suggests partial positive charge on the hydrogen atom indicating its H-bond donor character. On the other hand, in the case of MA unit, the oxygen atom juxtaposed between the two carbonyl groups can only act as H-bond acceptor as it shows negative MESP mainly arising from its lone pair electrons.

*3.2.1.2. Microsolvation of **1** and **2**.* The interaction of **1** and **2** with a maximum of three water molecules is studied by modeling the structures **1**···(H_2O), **1**···(H_2O)$_2$, **1**···(H_2O)$_3$, **2**···(H_2O), **2**···(H_2O)$_2$, and **2**···(H_2O)$_3$. The optimized structures are presented in Fig. 7. The H-bond interactions in the systems are shown by dotted lines. As we can see, the hydration pattern of **1** is markedly different from that of **2**. In the case of **1**, even a single water molecule can interact simultaneously with carbonyl oxygen and the N–H hydrogen. The water dimer and trimer are interacting with the carbonyl oxygen/s and the N–H hydrogen of **1** via a network of well defined H-bonds. Since there is no strong H-bond donor in **2**, its main H-bond interaction is through the carbonyl oxygen and the remaining interactions are found to be with the hydrophobic C–H bonds. The H-bond interactions through C–H bonds are expected to be very weak as they show H-bond distances in the range of 2.700–2.836 Å. It may be noted that in **2**···(H_2O)$_3$, one would expect the participation of the second carbonyl group in the H-bond interaction. In fact, the initial structure for the optimization was selected in such a way that all the three oxygen atoms show H-bond interactions with water molecules. However, the

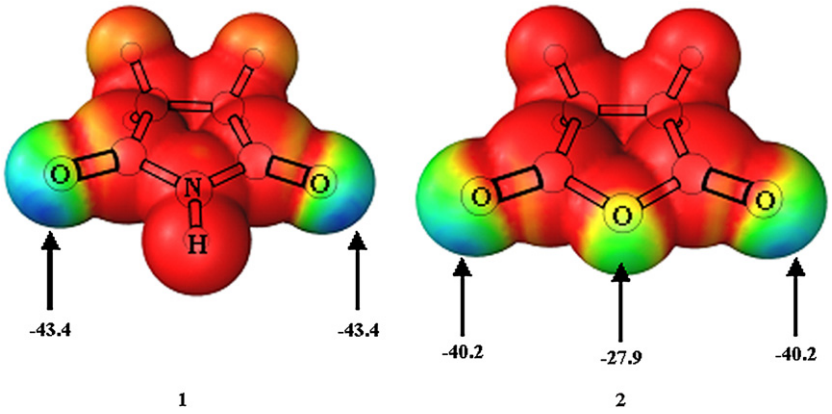

Fig. 6. Molecular electrostatic potential plotted on the van der Waals surface of **1** and **2**. Color coding ( ) from red to blue is +62.7 to −12.6 kcal/mol. All values in kcal/mol. (For interpretation of the references to color in this figure legend, the reader is referred to the web version of this article.)

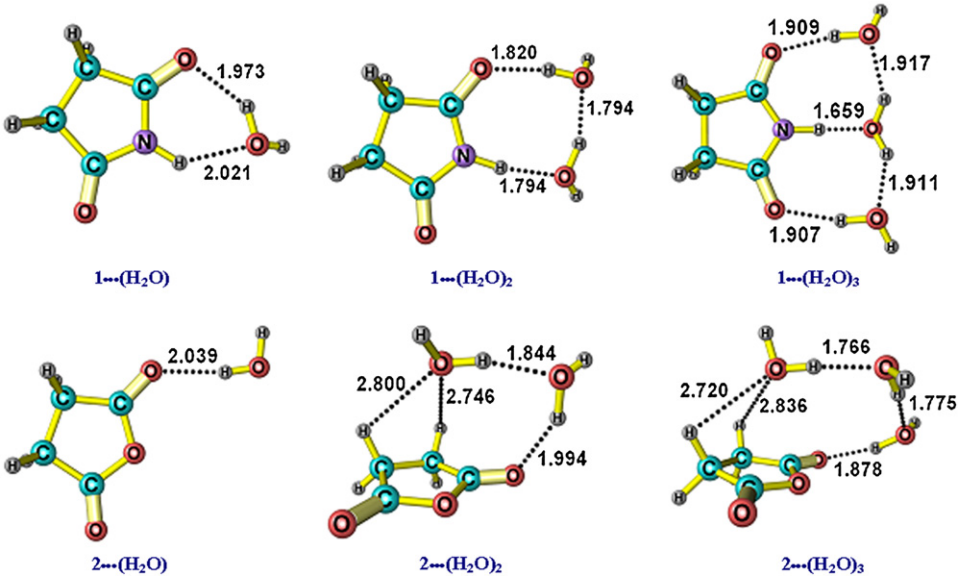

Fig. 7. Optimized structures of microsolvated structures of **1** and **2**. The dotted lines are intramolecular H-bonds which showed a (3, −1) bond critical point in Bader's atoms in molecule theory.

optimization eventually led to the formation of the structure presented in Fig. 7. Further, even with four water molecules the H-bond interaction with the second carbonyl group was not obtained and therefore, we expect that more number of water molecules are required for the complete coverage of the two carbonyl groups as the anhydride moiety can only act as H-bond acceptor.

The BSSE-corrected interaction energy values are calculated for all the microsolvated structures using the supermolecule approach (Table 3). The microsolvated systems of **1** always show more interaction energy than the corresponding systems of **2**. In the case of microsolvated systems of **1**, viz. **1**···(H_2O), **1**···(H_2O)$_2$, and **1**···(H_2O)$_3$, the calculated total H-bond interaction energy is 8.43, 18.59, and 28.26 kcal/mol, respectively. In comparison with these values, the microsolvated structures of **2** showed smaller values, viz. 3.49, 13.96, and 24.03 kcal/mol for **2**···(H_2O), **2**···(H_2O)$_2$, and **2**···(H_2O)$_3$, respectively. Although it appears that **1** has more hydration power than **2**, the energetics noted in Eqs. (1) and (2) suggest that on going from **2**···(H_2O) to **2**···(H_2O)$_2$ or **2**···(H_2O)$_2$ to **2**···(H_2O)$_3$, the energy released is higher compared to the corresponding processes involving microsolvated systems of **1**.

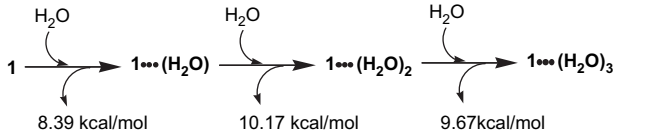

(1)

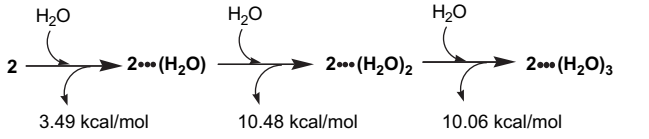

(2)

Table 3
Total H-bond energy and the H-bond distances in microsolvated **1** and **2**

System	Total H-bond energy (kcal/mol)	H-bond distance (Å)
1···(H_2O)	−8.43	1.973
		2.021
1···(H_2O)$_2$	−18.59	1.820
		1.794
		1.794[a]
1···(H_2O)$_3$	−28.26	1.909
		1.659
		1.907
		1.917
		1.911
2···(H_2O)	−3.49	2.039
2···(H_2O)$_2$	−13.96	1.994
		1.844
		2.746
		2.800
2···(H_2O)$_3$	−24.03	1.766
		1.775
		1.878
		2.720
		2.836

[a] H-bond between the two water molecules.

We have also analyzed the following equations:

$$\mathbf{1} + (H_2O)_2 \rightarrow \mathbf{1}\cdots(H_2O) + H_2O \quad (3)$$

$$\mathbf{2} + (H_2O)_2 \rightarrow \mathbf{2}\cdots(H_2O) + H_2O \quad (4)$$

$$\mathbf{1} + (H_2O)_3 \rightarrow \mathbf{1}\cdots(H_2O)_2 + H_2O \quad (5)$$

$$\mathbf{2} + (H_2O)_3 \rightarrow \mathbf{2}\cdots(H_2O)_2 + H_2O \quad (6)$$

$$\mathbf{1} + (H_2O)_4 \rightarrow \mathbf{1}\cdots(H_2O)_3 + H_2O \quad (7)$$

$$\mathbf{2} + (H_2O)_4 \rightarrow \mathbf{2}\cdots(H_2O)_3 + H_2O \quad (8)$$

In these equations, (H_2O)$_2$, (H_2O)$_3$, and (H_2O)$_4$ are the dimer, trimer and tetramer of systems of water molecule (Fig. 8). Therefore, Eq. (3) suggests that when **1** interacts with a water dimer, it knocks of one water molecule to form the **1**···(H_2O) system. Similar interpretations can be made for Eqs. (4)–(8). The reactions involving **1** given in Eqs. (3) and (5) are found to be exothermic by 3.23 and 2.53 kcal/mol, respectively, and reaction given in Eq. (7) is nearly thermo neutral as it is endothermic by only 0.17 kcal/mol. However, all the reactions involving **2** are found to be endothermic by 1.70, 2.09, and 4.41 kcal/mol for Eqs. (4), (6) and (8), respectively. The exothermic character observed for reactions of **1** suggests its hydrophilic character while the endothermic reactions of **2** are in agreement with its hydrophobic character. It may be noted that both **1** and **2** interacting with only one water molecule are exothermic by 8.39 and 3.49 kcal/mol, respectively. It means that the free moving water molecules account mainly for the hydration of **2**.

*3.2.1.3. Structures of **3** and **4**.* Structures of **3** and **4** are models corresponding to a small section of the NIPAM-*co*-MI and NIPAM-*co*-MA copolymers, respectively. The optimized structure of these systems is presented in Fig. 9. Structure of **3** is characterized by an intramolecular C═O···H−N H-bond of length 2.171 Å. This bonding gives a bend −C−C−C− backbone. On the other hand, the most stable structure of **4** has got no such intramolecular H-bond and therefore its structure is more linear than the structure of **3**. In fact, in the case of **4**, a bend structure (**4′**) similar to **3** (with an intramolecular H-bond) is found to be 2.01 kcal/mol less stable than the linear structure. The H-bond length of **4′** (2.345 Å) is longer than the H-bond length of **3**, which indicates that H-bond interaction in the former is weaker than that in the latter system. It is apparent that the energy required for the bending of **4** leading to **4′** is not completely compensated by the intramolecular H-bond, whereas **3** is more inclined towards a bend structure (in the case of **3**, a linear structure was absent as an optimization starting from a linear structure gave the same bend structure shown in Fig. 9). The above features of **3** and **4** are interesting because they suggest that NIPAM-*co*-MI based polymer has got an inherent tendency towards more bended

or folded form compared to the NIPAM-*co*-MA based polymer.

*3.2.1.4. Interaction of H_2O with **3** and **4**.* The interaction of a water molecule with **3** and **4** is also considered by optimizing the structures **3**···(H_2O) and **4**···(H_2O) (Fig. 10). Structure **3**···(H_2O) showed an H-bond interaction energy of 9.74 kcal/mol whereas a slightly higher value of 9.82 kcal/mol is obtained for **4**···(H_2O).

*3.2.1.5. Dimers of **3** and **4**.* In the dimer of **3** (**3**···**3**), two strong intermolecular H-bond interactions of the type N–H···O=C with nearly equal strength are present (Fig. 11). Structure **3**···**3** is also stabilized by weak intermolecular C–H···O=C type and intramolecular N–H···O=C type interactions. The BSSE-corrected dimerization energy is found to be 9.64 kcal/mol.

In the case of dimer of **4** (**4**···**4**), two N–H···O=C type H-bonds with same distance (2.094 Å) are present (Fig. 11). In **4**···**4**, the intramolecular N–H···O=C bond is absent while two weak intermolecular C–H···O=C interactions are present. It may be noted that the presence of intramolecular N–H···O=C bond in **3**···**3** gives a puckered or a more folded structure while the absence of this type of bond in **4**···**4** leads

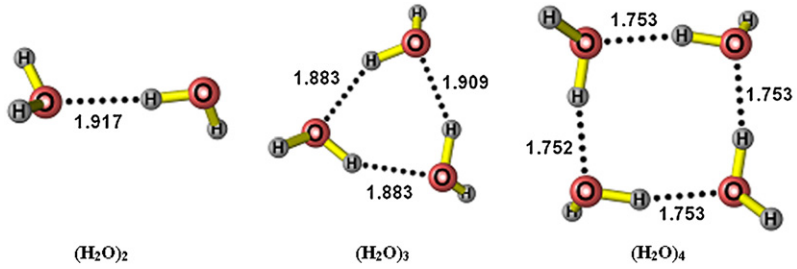

Fig. 8. Optimized structures of water dimer, trimer, and tetramer.

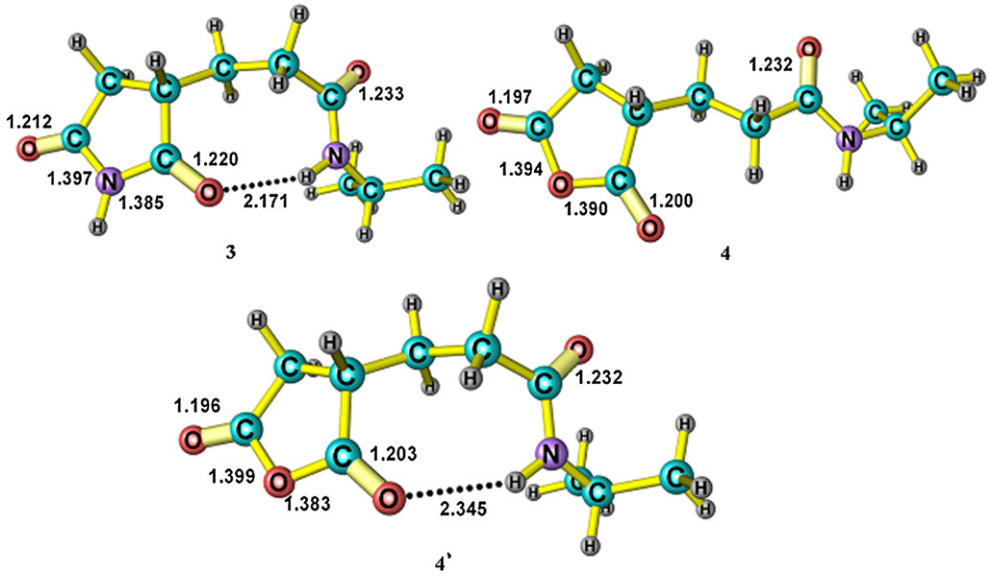

Fig. 9. Optimized structures of **3**, **4**, and **4′** showing the intramolecular H-bond interaction.

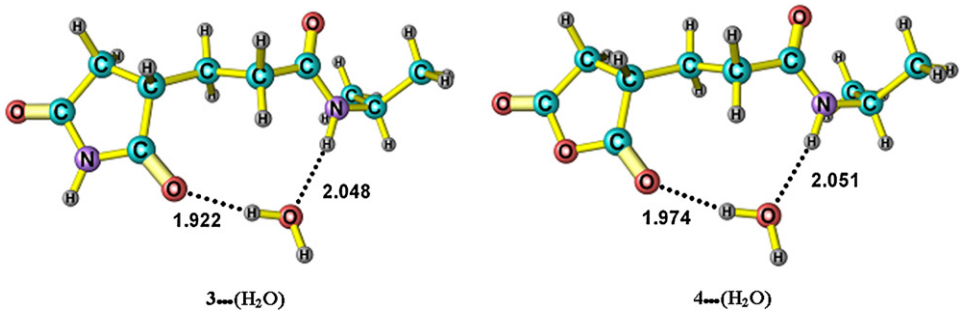

Fig. 10. Optimized structures of **3**···(H_2O) and **4**···(H_2O) showing the intermolecular H-bond interactions.

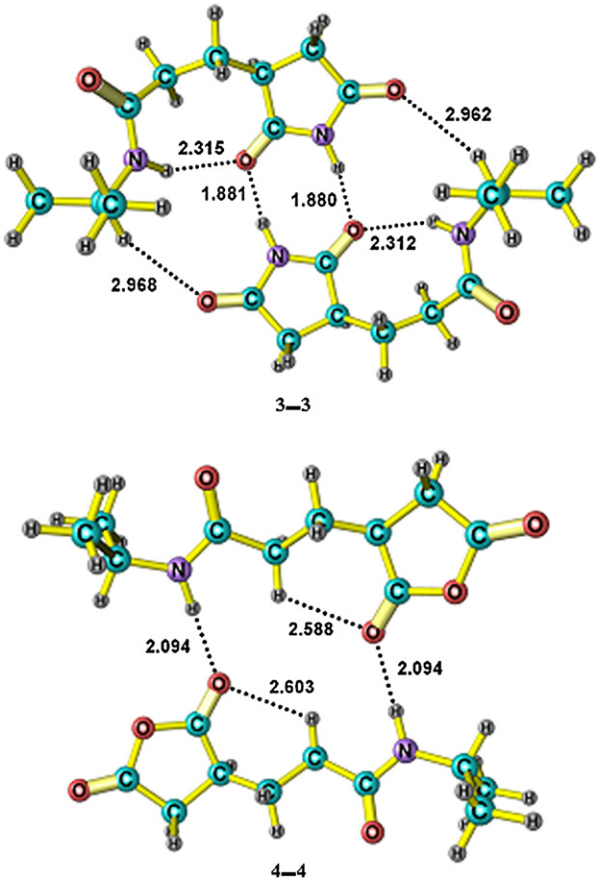

Fig. 11. Optimized structures of dimers of **3** and **4** showing inter- and intramolecular H-bonds.

to a more flat structure. For instance the N to N distance of **3** in **3**···**3** is 5.097 Å whereas the N to −O− distance of **4** in **4**···**4** is 6.736 Å. The BSSE-corrected interaction energy in **4**···**4** is found to be 8.42 kcal/mol. The interaction energy analysis suggests that the formation of the dimer system **3**···**3** is more stable than the **4**···**4** dimer.

Based on the theoretical results presented in this work, we can say that the MI based systems have a higher tendency for hydration than the MA based systems. On the other hand, the MI based systems have an inherent nature for the formation of a bend structure due to intramolecular H-bond (Fig. 9) while the MA based systems are likely to adopt more linear structures due to the absence such H-bonds. Further, compared to the MA unit, the H-bond donating and accepting character of MI unit is suitable for the easy formation of its dimer structures (Fig. 11). It may be noted that in the case of MI based systems, the hydration is mostly an exothermic process whereas in the case MA based systems one would expect endothermic character for the hydration when interact with water clusters (Eqs. (1)−(8)). However, the interaction of MA unit with free moving water molecules is an exothermic process, which suggests that a rise in the temperature may enhance the hydration of the MA based system. Therefore, the LCST behavior presented in Fig. 3 for poly(NIPAM-*co*-MI) and poly(NIPAM-*co*-MA) can be mainly understood in terms of the hydration and the folding behavior of these polymers at their MI and MA regions. By increasing the percentage of MI units in the polymer, the dimeric MI···MI interaction is going to increase. This in turn will lead to more folded polymeric structures and thereby a decrease in the direct MI···(H_2O) interactions is expected. In the case of poly(NIPAM-*co*-MA) systems, the MA units will be more exposed to the solvent because of its less tendency towards the formation of folded structures with MA···MA interactions. Therefore, an increase in the MA percentage in the polymer can increase the MA···(H_2O) interactions. Further, a rise in temperature can also enhance the hydration power of MA unit.

3.2.2. Molecular dynamic simulation

To enhance our knowledge on the hydration behavior of the copolymers and the associated LCST behavior, classical molecular dynamic simulations have been carried out on oligomer models. For this purpose, we have created 50-unit oligomer chains of both the copolymers containing 20% of MA and MI in a random atactic manner [10]. The partial charges of the atoms of the whole chains were found by using Mulliken charge separation method with a semiempirical PM3 wavefunction [24]. By using the TIP3 water model containing 10,000 molecules, the chains were solvated to make a dilute solution, comparable to the experimental conditions. The all atom AMBER force field [25] was used to describe the inter- and intramolecular interactions. NPT simulations at $P = 1$ atm were performed using the sander module of AMBER 9 [26]. A 10 Å cut-off and Ewald sums were used for the non-bonded interactions. The SHAKE [27] algorithm was used to constrain the bond lengths involving hydrogen atoms.

In Fig. 12, a 1 ns MD simulation in vacuum is presented in the case of the oligomer system constructed for NIPAM-*co*-MI at two different temperatures, viz. one at the LCST (290 K) and the other above the LCST (310 K). For both the simulations, unfolded structures were used at the beginning and the final structure was turned out to be highly folded through intramolecular hydrogen bonding with no considerable change in the system configurations equilibrated at either temperatures. Very similar observations are also obtained for the oligomer model of NIPAM-*co*-MA. Thus we expect extensive change in the configurations in water because of the water−solute intermolecular hydrogen bonding competing with the intramolecular hydrogen bonding. Analogous MD simulation results conducted on oligomer model of NIPAM can be seen in the work of Fornili et al. [10].

In the next step, a 4 ns NPT MD simulations at 290 and 310 K was conducted for both the oligomer chains in about 10,000 TIP3 water molecules (prior to the full simulations, the structures were equilibrated at the respective temperatures for 20 ps). The oligomer structural changes occurring along these simulations were monitored through the radius of gyration of the solute, whose time evolutions are depicted in Fig. 13.

The radius of gyration studies show that NIPAM-*co*-MA has relatively similar configurations at both the temperatures

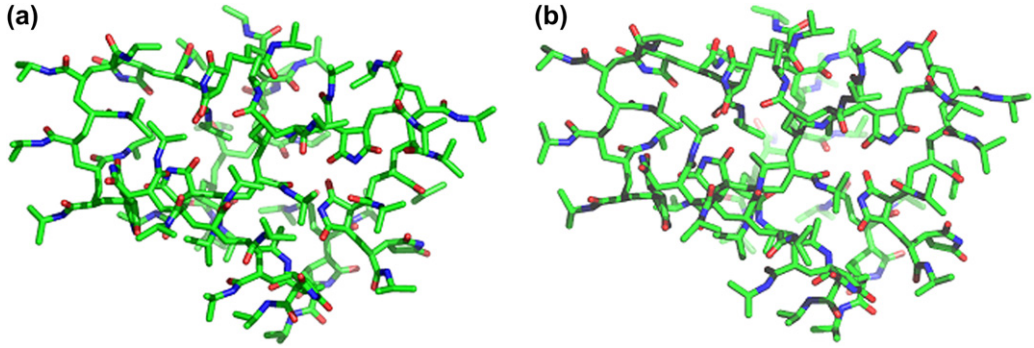

Fig. 12. The final optimized structures of NIPAM-*co*-MI after 1 ns MD simulation at (a) 290 K and (b) 310 K. For clarity hydrogen atoms are omitted.

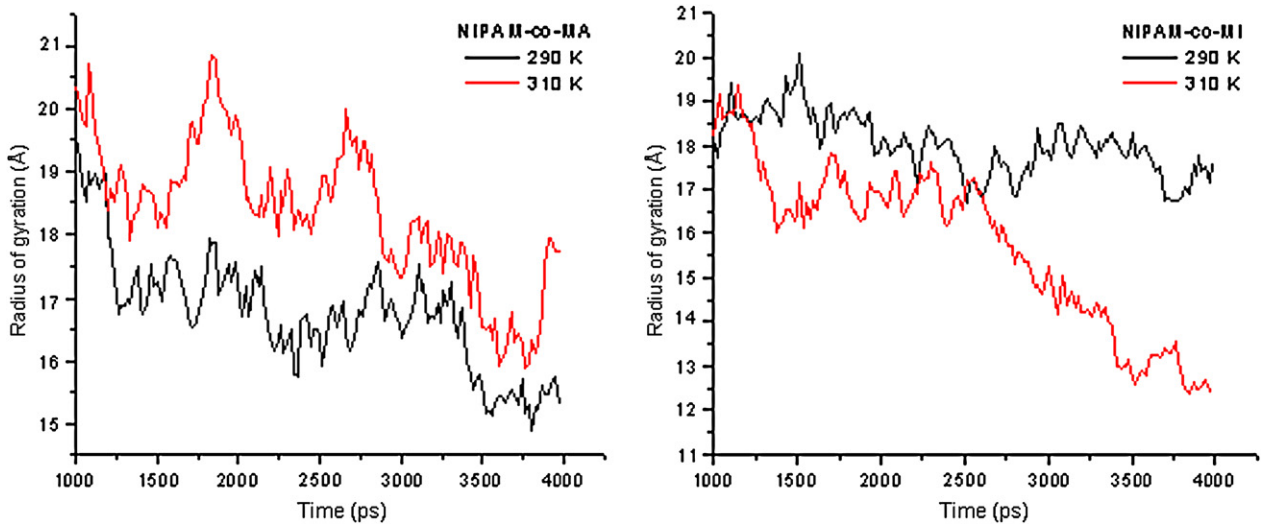

Fig. 13. Time evolution of radius of gyration along the MD simulations of (a) NIPAM-*co*-MA and (b) NIPAM-*co*-MI oligomers in water at 290 and 310 K, respectively.

and NIPAM-*co*-MI attains a compact configuration at 310 K. Also it can be noted that the radius of gyration has almost equal values at some places, but the trajectory analysis showed that the structures are entirely different. Further, it may be seen that some regions of the oligomer chain remain persistent throughout the simulations and the hydrogen bond analysis showed that such structural features arise due to the intrachain hydrogen bonding. From Figs. 14 and 15, the folding nature at the higher and lower temperatures can be clearly understood. NIPAM-*co*-MI has a clear coil to globule transition (Fig. 14a and b) at the higher temperature while the NIPAM-*co*-MA system offers more resistance towards such a transition. The absence of globule formation in NIPAM-*co*-MA can be due to the repulsion between the oxygen atoms in the nearby MA rings. The fluctuations in the radius of gyration curve can also be explained in this manner.

The hydrogen bond analysis revealed that at all temperatures the number of intrachain hydrogen bonds as well as the number of water–solute hydrogen bonds are more in the case of NIPAM-*co*-MI than NIPAM-*co*-MA. However, when compared with NIPAM, it was found that the intrachain hydrogen bonding was lesser in both the copolymers. This can be due to the structural rigidity of the chain due to the presence of the five-membered rings.

The data that the number of water molecules within the first solvation shell (<3.5 Å) decreasing at higher temperature (Fig. 16) are also a proof for the coiling of the oligomer chain. This points out that the surface of the oligomer chain accessible to the solvent decreases at higher temperature. It is clear from Fig. 6 that the decrease in the number of water molecules is greater for NIPAM-*co*-MI than for NIPAM-*co*-MA. The hydrogen bond data also revealed that at 290 K, the intrachain hydrogen bond is between the adjacent monomer units as in Fig. 11, whereas at higher temperature the nonadjacent hydrogen bonds become more and more persistent and these bonds remain stronger throughout the remaining part of the dynamics.

4. Conclusions

In this work, the synthesis and characterization of NIPAM-*co*-MI are reported. Further, thermo-sensitive nature of this copolymer was compared with that of NIPAM-*co*-MA, which

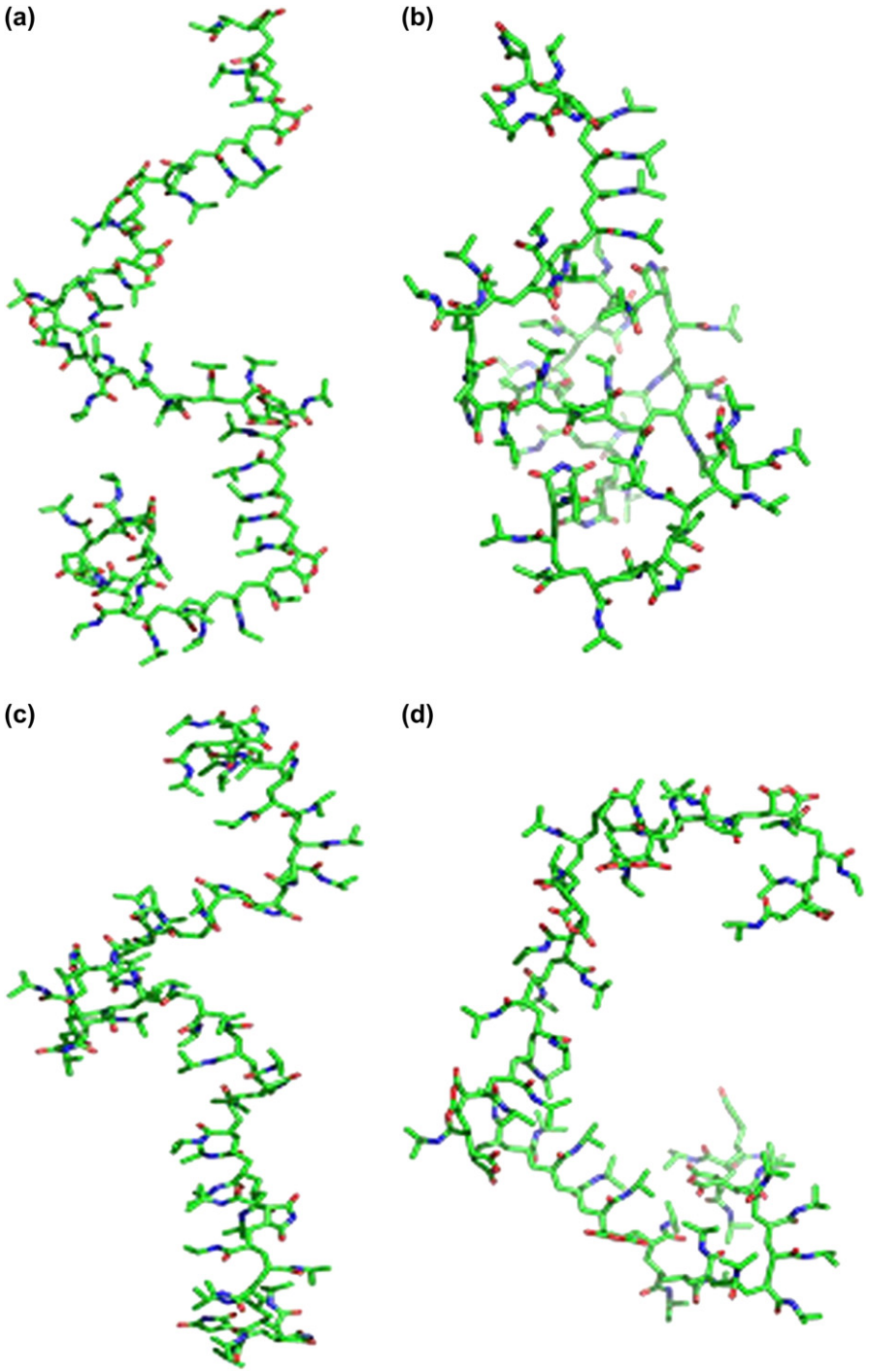

Fig. 14. Initial (a), (c) and final (b), (d) configurations in the 4 ns MD simulations of NIPAM-*co*-MI and NIPAM-*co*-MA oligomer units, respectively, in aqueous solution at 310 K. For clarity, hydrogen atoms are omitted.

was reported earlier. In the latter case, a rise in LCST with increase in MA loading in the polymer is observed whereas in the case of NIPAM-*co*-MI, the LCST lowered with increase in the MI units. This was partially addressed by comparing the hydration pattern and the possibility of H-bond interactions around the repeat unit in both the systems by DFT level quantum mechanical (QM) calculations on small models. The QM models showed that the MI based polymer is more inclined towards bend structure, higher hydration, and higher intramolecular hydrogen bond formation between its monomer units when compared to those of the MA based polymer. The QM results were augmented with the data obtained from large scale classical MD simulations carried out on large oligomer models of the systems at the LCST and above LCST temperatures. The MD simulations were carried out for 4 ns using 50-unit oligomers of NIPAM-*co*-MA and NIPAM-*co*-MI in about 10,000 TIP3 water molecules. The trajectory analysis showed that at higher temperature, the oligomers

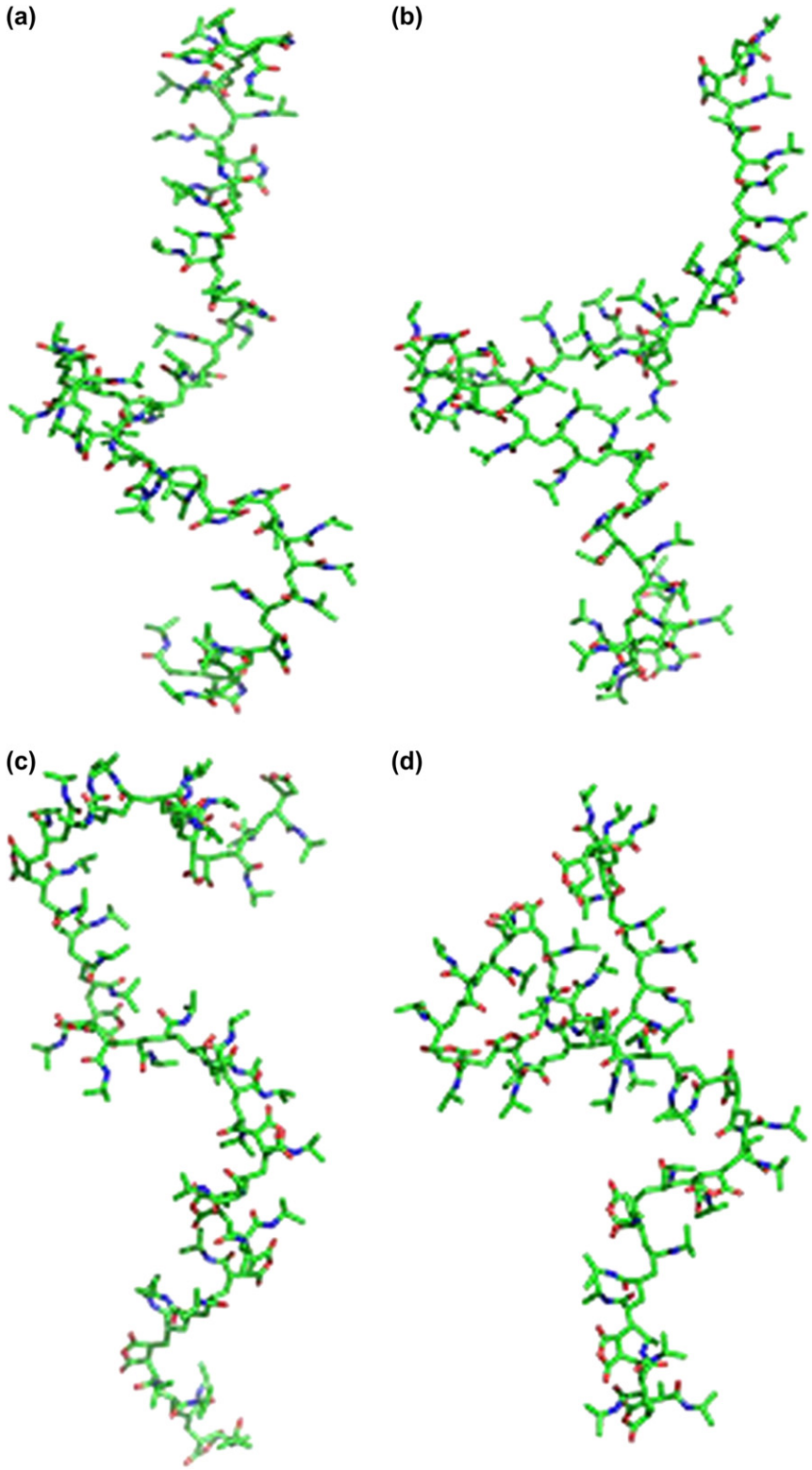

Fig. 15. Initial (a), (c) and final (b), (d) configurations in the 4 ns MD simulations of NIPAM-*co*-MI and NIPAM-*co*-MA oligomer units, respectively, in aqueous solution at 290 K. For clarity, hydrogen atoms are omitted.

have a more compact structure due to extensive intrachain hydrogen bonds. The radius of gyration and hydrogen bonding data were clearly in accordance with the expected folding behavior of the two copolymers. Also it was found that the water molecules stabilize the oligomer chains by extensive hydrogen bonding. Thus it can be concluded that a change from anhydride to imide reversed the LCST of NIPAM copolymer which is attributed mainly to difference in intrachain hydrogen bonding ability, hydration and folding behavior of the two copolymers.

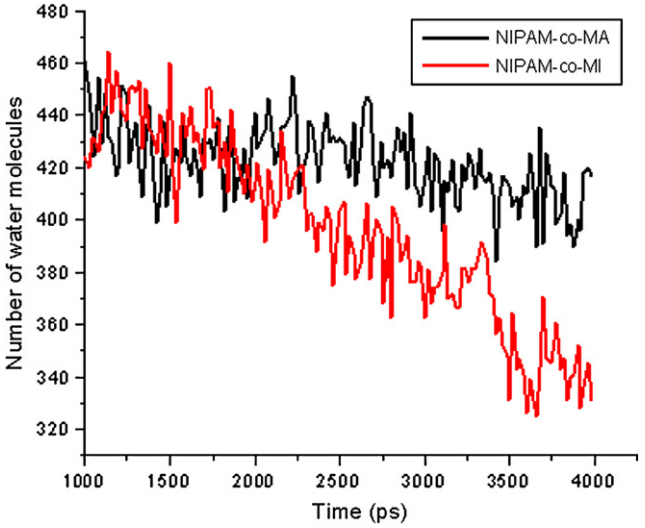

Fig. 16. The time evolution of the number of water molecules in the first solvation shell (<3.5 Å) of both oligomer chains at 310 K.

Acknowledgments

With great pleasure the author (R.F.) acknowledges the financial support received from Department of Science and Technology (DST-FT Scheme No. SR/FTP/**CSA-17**/2003), Government of India. C.H.S. gratefully acknowledges the support from the high performance computing facility of IGIB, New Delhi for doing the AMBER simulations.

References

[1] (a) Schild HG. Prog Polym Sci 1992;17:163;
(b) Walker JA, Vause CA. Sci Am 1987;253:98;
(c) Tager A. Physical chemistry of polymers. Moscow: Mir; 1972.
[2] Schild HG, Tirrel DA. J Phys Chem 1990;94:4352.
[3] (a) Yoshida R, Sakai T, Okano T, Sakurai Y, Bae YH, Kim SW. J Biomater Sci Polym Ed 1991;3:155;
(b) Cammas S, Suzuki K, Sone Y, Kakurai Y, Kataoka K, Okano T. J Controlled Release 1997;48:157;
(c) Kono K. Adv Drug Delivery Rev 2001;53:307;
(d) Kwon IC, Bae YH, Kim SW. Nature 1991;354:291.
[4] Feil H, Bae YH, Feijen J, Kim SW. Macromolecules 1993;26(10):2496.
[5] Weng Y, Ding Y, Zhang G. J Phys Chem B 2006;110:11813.
[6] Bergbreiter DE. Chem Rev 2002;102:3345.
[7] Graziano G. Int J Biol Macromol 2000;27:89.
[8] Anfinsen C. Biochem J 1972;128(4):737.
[9] Kesim H, Rzaev ZMO, Dincer S, Piskin E. Polymer 2003;44:2897.
[10] Longhi G, Lebon F, Abbate S, Fornili SL. Chem Phys Lett 2004;386:123.
[11] Tawney PO, Snyder RH, Bryan CE. J Org Chem 1960;25:56.
[12] Jia X, Pang Y, Huang J. J Polym Sci Part A Polym Chem 1998;36:1291.
[13] Koseli V, Rzaev ZMO, Piskin E. J Polym Sci Part A Polym Chem 2003;41:1580.
[14] Lee C, Yang W, Parr RG. Phys Rev B 1988;37:785.
[15] Becke AD. J Chem Phys 1993;98:5648.
[16] Politzer P, Truhlar DG. Chemical applications of atomic and molecular electrostatic potentials. New York: Plenum; 1981.
[17] Gadre SR, Shirsat RN. Electrostatics of atoms and molecules. Hyderabad: Universities Press; 2000.
[18] Hobza P, Zahradnyik R. Chem Rev 1988;88:871.
[19] (a) Boys SF, Bernardi F. Mol Phys 1970;19:553;
(b) Frisch MJ, Trucks GW, Schlegel HB, Scuseria GE, Robb MA, Cheeseman JR, et al. Gaussian 03 Revision C.02. Wallingford CT: Gaussian Inc; 2004.
[20] Suresh CH, Koga N, Gadre SR. J Org Chem 2001;66:6883.
[21] Suresh CH, Gadre SR. J Am Chem Soc 1998;120:7049.
[22] Suresh CH. Inorg Chem 2006;45:4982.
[23] Suresh CH, Koga N. Inorg Chem 2002;41:1573.
[24] Stewart JJP. J Comput Chem 1989;10:221.
[25] Cornell WD, Cieplak P, Bayley CI, Gould IR, Merz Jr KM, Ferguson DM, et al. J Am Chem Soc 1995;117:5179.
[26] Case DA, Darden TA, Cheatham III TE, Simmerling CL, Wang J, Duke RE, et al. AMBER 9. San Francisco: University of California; 2006.
[27] Miyamoto S, Kollman PA. J Comput Chem 1992;13:952.